ACS APPLIED MATERIALS & INTERFACES

Research Article

www.acsami.org

Demonstration of Resonance Coupling in Scalable Dielectric Microresonator Coatings for Photovoltaics

Dongheon Ha,[†,‡] Chen Gong,[‡,§] Marina S. Leite,[‡,§] and Jeremy N. Munday*[,†,‡]

[†]Department of Electrical and Computer Engineering, University of Maryland, College Park, Maryland 20742, United States
[‡]Institute for Research in Electronics and Applied Physics, University of Maryland, College Park, Maryland 20742, United States
[§]Department of Materials Science and Engineering, University of Maryland, College Park, Maryland 20742, United States

Supporting Information

ABSTRACT: To increase the power conversion efficiency of solar cells, improved antireflection coatings are needed to couple light into the cell with minimal parasitic loss. Here, we present measurements and simulations of an antireflection coating based on silicon dioxide (SiO_2) nanospheres that improve solar cell absorption by coupling light from free space into the absorbing layer through excitation of modes within the nanospheres. The deposited monolayer of nanospheres leads to a significant increase in light absorption within an underlying semiconductor on the order of 15−20%. When the periodicity and spacing between the nanospheres are varied, whispering gallery-like modes can be excited and tuned throughout the visible spectrum. The coating was applied to a Si solar cell containing a Si_3N_4 antireflection layer, and an additional increase in the spectral current density of ∼5% was found. The fabrication process, involving Meyer rod rolling, is scalable and inexpensive and could enable large-scale manufacturability of microresonator-based photovoltaics.

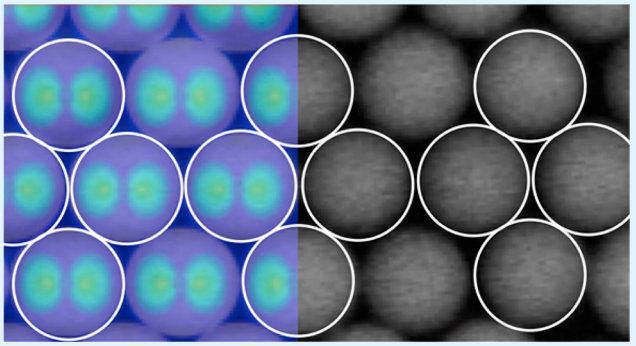

KEYWORDS: *whispering gallery modes, absorptivity enhancement, photocurrent enhancement, microresonator, antireflection coatings*

INTRODUCTION

To date, many methods have been applied to reduce reflection in photovoltaic (PV) devices, including single- and double-layer thin-film coatings,[1−4] plasmonic effects,[5−17] Mie resonances,[18,19] dielectric microstructures,[20−27] surface texturing,[28] etc. However, most of these antireflection coatings (ARCs) are manufactured by film deposition techniques such as chemical vapor deposition (CVD), sputtering, or evaporation (as well as possible lithography steps), which are costly and often involve high-temperature environments that are unsuitable for certain solar cell technologies. Recently, flexible and environmentally friendly ARCs based on cellulose materials, which do not require these vacuum-based or high-temperature fabrication processes, have been introduced.[29,30] Nevertheless, more research on the durability of these coatings is necessary to determine their applicability as commercial ARCs.

Silicon dioxide (SiO_2) nanospheres offer a promising nanophotonic ARC option due to their light trapping and scattering properties.[20−22] Further, SiO_2 nanoscale structures can overcome most of the above-mentioned difficulties as they are stable with respect to extreme temperatures and illumination. Moreover, SiO_2 is earth abundant. Different techniques have been used to achieve layers of SiO_2 nanospheres on top of photoactive layers on flexible and rigid substrates, including the Langmuir−Blodgett method,[22,31] sedimentation,[32] and controlled evaporation.[33] Despite the success in obtaining large areas covered with spheres, these approaches are not generally compatible with roll-to-roll processes, which are required for most continuous, mass production approaches.

The Meyer rod rolling technique has been used to deposit solution-based nanomaterials (i.e., graphene,[34] silver nanowires,[35] and carbon nanotubes[36]) on a variety of mechanical supports, including plastics, wafers, and glasses, enabling coatings for flexible electronics and energy storage devices. Here, we use the Meyer rod rolling technique with an aqueous solution containing SiO_2 nanospheres and demonstrate that optical modes can be excited from incident illumination and lead to increased photocurrent in an underlying solar cell.

RESULTS AND DISCUSSION

We present an effective and potentially scalable ARC for PV based on SiO_2 dielectric nanospheres deposited by the Meyer rod rolling technique, which produces broadband absorptivity enhancement of >15% when applied to Si solar cells. The highly periodic configuration of the SiO_2 nanospheres leads to

Received: May 13, 2016
Accepted: August 24, 2016
Published: August 24, 2016

DOI: 10.1021/acsami.6b05734
ACS Appl. Mater. Interfaces 2016, 8, 24536−24542

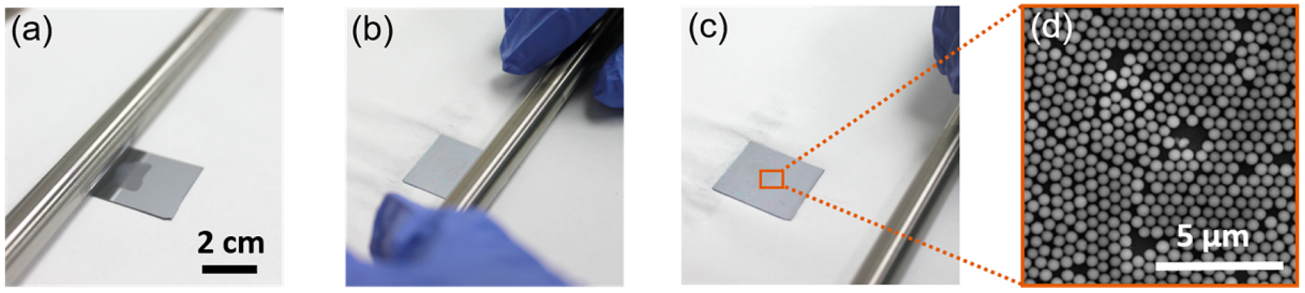

Figure 1. (a–c) Photographs depicting the fabrication steps for the SiO_2 dielectric nanosphere coating on top of a c-Si wafer. A Meyer rod is pulled along the surface of a Si wafer with a droplet of suspension containing SiO_2 nanospheres. The sample is then submitted to a mild annealing treatment at 50 °C for 1 min for water evaporation. (d) SEM image showing one monolayer of SiO_2 nanospheres on a Si substrate.

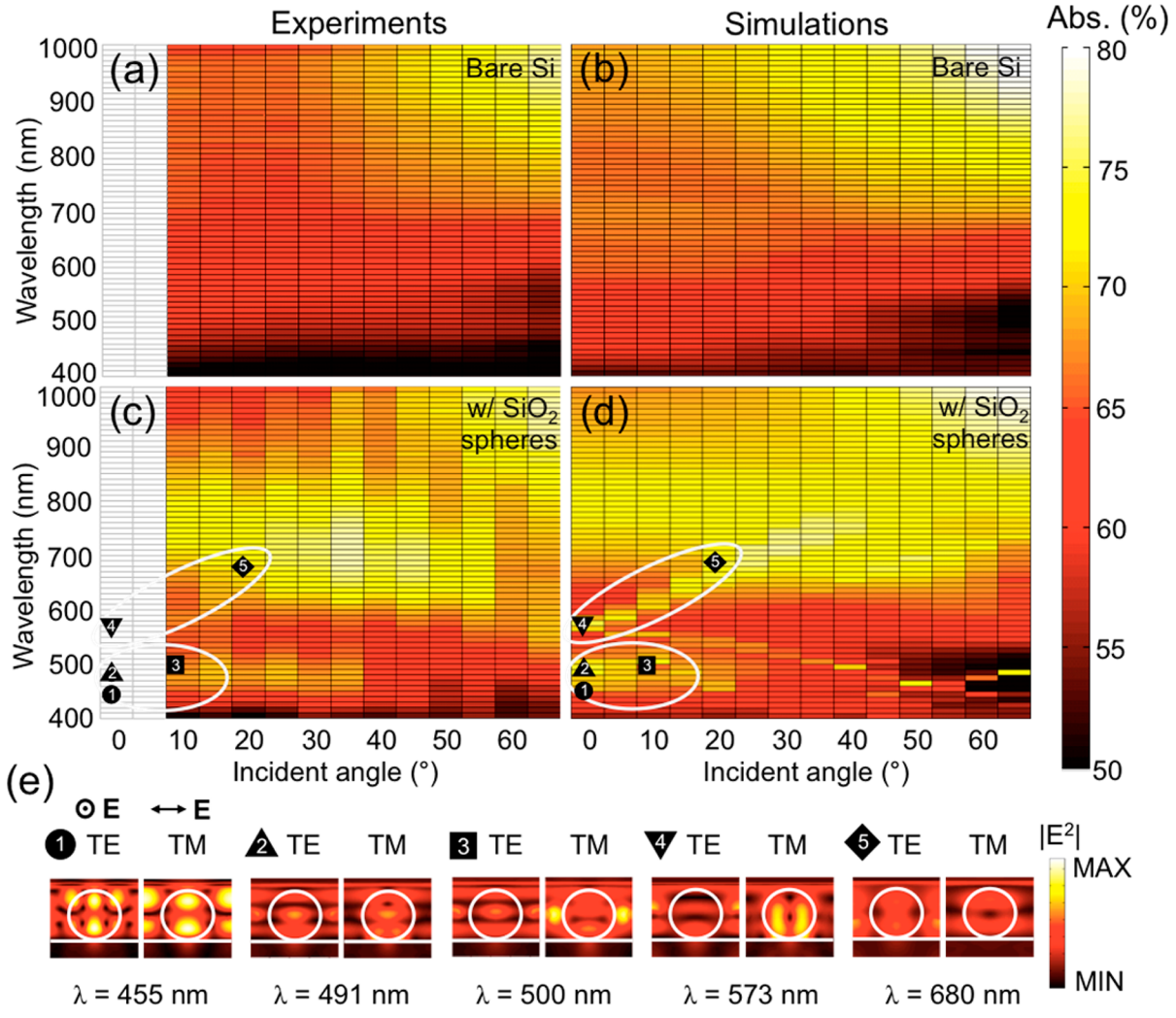

Figure 2. Contour plots showing (a and c) experimental and (b and d) simulated absorptivity as a function of both wavelength (λ = 400–1000 nm) and angle of incidence (θ = 0–65°) of incoming light for (a and b) a bare Si wafer and (c and d) a Si wafer with a close-packed monolayer of SiO_2 nanospheres. All calculations are based on the FDTD method. There is no experimental data for incident angles <10° due to geometric constraints that are typical to integrating sphere systems. (e) Electric field profiles for data points numbered 1–5 in panels c and d are shown for each incident polarization. Illumination angle is defined as the angle between the surface normal and the direction of incident light.

the excitation of particular optical modes within the structure, which produces distinct electric field distributions that strongly indicate the presence of whispering gallery-like modes within the nanospheres.

Here, we employ a water-based process to assemble a monolayer of SiO_2 nanospheres on a substrate by the Meyer rod rolling technique, which produces close-packed arrays with high-density coverage. To generate a close-packed monolayer of SiO_2 nanospheres, a surfactant (Zonyl) is added to the nanosphere suspension to prevent aggregation. The suspension containing nanospheres is then spread on the top of a semiconducting substrate, and a dense monolayer of SiO_2 nanospheres assembles during the drying process (see the Methods Section for details). Figures 1a–c shows the steps

DOI: 10.1021/acsami.6b05734
ACS Appl. Mater. Interfaces 2016, 8, 24536–24542

required to obtain a close-packed monolayer of spheres with diameters of 500 nm and a coverage area of ~67%, as shown in Figure 1d and discussed in the Supporting Information. This coverage can be improved through further optimization of the coating technique; however, the achieved coverage is sufficient to demonstrate the optical resonances, as presented later in the article.

The SiO_2 nanosphere ARC results in increased absorption throughout the solar spectrum, as determined from experiments (Figure 2). An integrating sphere and monochromatic light were used to measure the absorptivity as a function of angle of incidence (θ = 10−65°) and wavelength (λ = 400−1000 nm) for both a bare Si reference wafer (Figure 2a) and a Si wafer with the nanosphere ARC (Figure 2c). The addition of the SiO_2 nanosphere layer leads to both broadband and narrowband absorption enhancements throughout the visible spectrum that vary with incident wavelength and illumination angle from the surface normal. One simple explanation for the increased absorption is that the spheres constitute a new thin-film layer that acts as an antireflection coating whose index of refraction varies with thickness based on the weighted-average of the index at each distance from the Si slab's surface (Supporting Information). This explanation accounts for the two broadband absorption enhancement regions that occur at ~500 and ~750 nm at normal incidence and shift to slightly shorter wavelengths for larger incident angles (Figure S1).

However, additional narrowband peaks (e.g., the absorption peak that occurs at ~600 nm in the experimental data for an incident angle of 10°, which shifts to longer wavelengths at higher angles) cannot be explained by this simple model. To better understand the origins of the narrowband resonances, simulations were performed using the finite-difference time-domain (FDTD) method, and contour plots of absorption were obtained (as a function of incident illumination wavelength and angle) for a thick Si slab with and without the nanosphere coating (Figures 2b and d). Simulations are performed for both polarizations to match the unpolarized light from the experiment. The simulations accurately describe the experimental data, including the absence of any sharp resonances for the bare Si. Figure 2d shows the calculated absorption in a Si slab with a close-packed layer of SiO_2 spheres, which is in good agreement with the experimental data shown in Figure 2c. In addition to the broadband absorption regions discussed above, the nanosphere coating also leads to regions with narrowband absorption, highlighted by white ellipses in Figures 2c and d.

Electric field intensities for each incident polarization (transverse magnetic (TM) and transverse electric (TE)) are displayed in Figure 2e for each numbered point in Figures 2c and d. The electric field profile of the TM incident light at point 4 (λ = 573 nm at normal incidence) strongly suggests the excitation of whispering gallery-like modes inside the sphere,[21,22] as confirmed by the field intensity profile (Figure 2e). These modes couple with each other, most likely due to the close proximity of the spheres, which allows for light scattering from one to another, ultimately leading to a significant increase in the electric field strength within the periodic array of nanospheres.[37−42] These enhanced fields then couple into the high-index absorbing material (Si wafer), leading to increased absorption in the Si.[23]

For an isolated SiO_2 nanosphere surrounded by an isotropic medium, we can describe the whispering gallery modes as electromagnetic modes with azimuthal variations, which are typically referred to as transverse electric or transverse magnetic depending on whether the electric or magnetic field is in the radial direction.[43] For an array of nanospheres above a substrate, we have asymmetries due to both the substrate and the adjacent spheres; however, for particular wavelengths, the field profiles resemble the fields of the whispering gallery modes of isolated spheres. For this reason, we refer to these resonances as whispering gallery-like modes.

To determine whether whispering gallery-like modes in each SiO_2 nanosphere actually couple into the Si absorbing layer, we probed the electric field intensity just inside the Si absorber. Figures 3a and b show the field intensity from normal incidence illumination at resonances 1 (λ = 455 nm) and 4 (λ = 573 nm), and Figure 3c shows the field intensity off resonance (λ = 600 nm). Resonances 1 and 4 (shown in Figure 2e) are not accessible with the experiment because they occur at normal incidence, but these resonances show a focusing effect (Figures

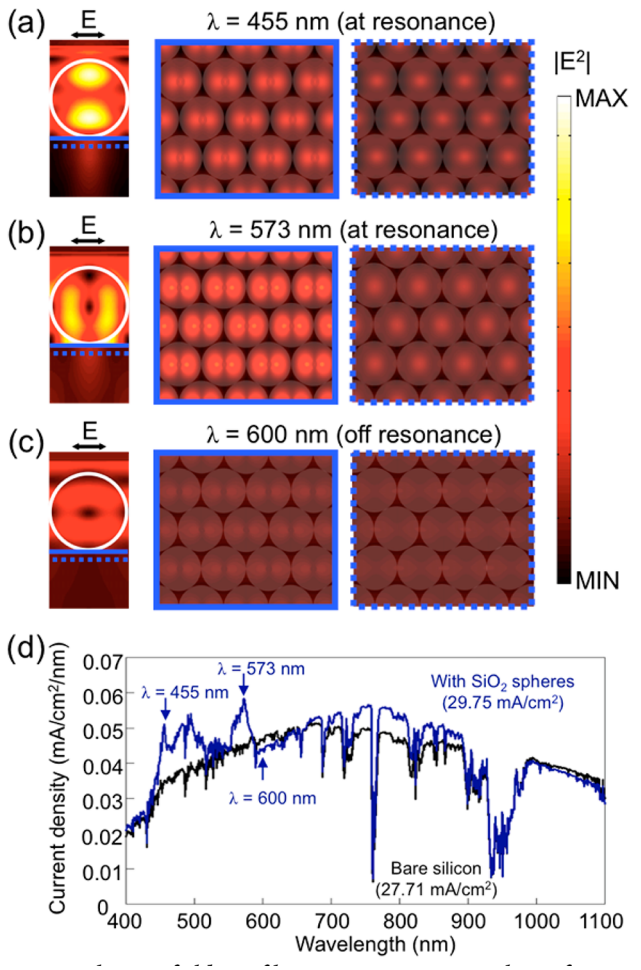

Figure 3. Electric field profiles at resonances resulting from illumination at (a) λ = 455 nm and (b) λ = 573 nm. High fields are observed inside the SiO_2 nanosphere which couple into the Si substrate. Lateral field profiles at the top of the Si substrate (blue solid line) and 50 nm below the interface (blue dotted line) show increased intensities within the Si for the resonant wavelengths (455 and 573 nm). (c) Electric field profiles for off-resonance illumination (λ = 600 nm), where no specific, strong field enhancements are observed. (d) Calculated spectral current density from two different structures: a bare Si cell (black) and a cell with close-packed SiO_2 nanospheres on top (blue). Enhancements in the spectral current density are observed at the wavelengths of 455 and 573 nm, and no enhancement is found at a wavelength of 600 nm.

DOI: 10.1021/acsami.6b05734
ACS Appl. Mater. Interfaces 2016, 8, 24536−24542

3a and b, left) that leads to increased semiconductor absorption. Figure 3b shows a whispering gallery-like mode with two high-intensity lobes, one on each side of the sphere, similar to the profile of the whispering gallery mode of an isolated sphere in an isotropic surrounding.[21] The electric field intensities both at the interface (blue solid line) and 50 nm below (blue dotted line) at resonances are much stronger than that of off-resonance excitation (Figure 3c, λ = 600 nm). As the index contrast between a nanostructure supporting a whispering gallery mode (e.g., nanosphere, nanodisk, nanocylinder, etc.) and its surrounding medium becomes larger, stronger optical mode confinement occurs within the nanostructure.[44] In our case, SiO_2 nanospheres are surrounded by air from above, and significant energy is captured inside the spheres. However, the light eventually leaks into the high-index absorbing substrate (i.e., Si wafer) beneath it, where it is absorbed due to evanescent coupling between the excited modes within nanostructures and the supporting structure (e.g., high-index absorbing substrate).[44,45]

To test the effect of the SiO_2 monolayer ARC on an optoelectronic device, we simulate the expected spectral current density of a solar cell with this coating (Figure 3d). To determine how much the current density is increased, the AM1.5G solar spectrum-weighted current density (J) was calculated for the cases with and without SiO_2 nanospheres atop the substrate (Figure 3d). The total current density was calculated based on the following expression:

$$J = q \int S(\lambda)\eta_{EQE}(\lambda)\mathrm{d}\lambda$$

where q is the electron charge, $S(\lambda)$ is the AM1.5G solar intensity per unit wavelength, and $\eta_{EQE}(\lambda)$ is the external quantum efficiency (EQE) of the device. For this calculation, $\eta_{EQE}(\lambda)$ is given by the absorptivity within the Si substrate assuming perfect internal quantum efficiency (IQE) for the wavelengths of interest in our calculation for simplicity. Figure 3d shows the calculated spectrally resolved current density. The absorptivity enhancement due to the previously described resonances (λ = 455 and 573 nm, Figures 3a and b) results in higher spectral current density. For a bare Si cell (black line), the total integrated current density (from λ = 400 nm to the bandgap of Si, λ = 1100 nm) is 27.71 mA/cm^2. With the addition of the close-packed SiO_2 nanosphere coating, the spectral current density (blue line) increases to 29.75 mA/cm^2, a ~ 7.4% improvement over that of a bare cell. As expected, the spectral current density at λ = 600 nm (off-resonance, Figure 3c) is much lower than the current density at either of the resonant peaks. Thus, we expect that this new ARC, yielding a high absorptivity enhancement, can significantly increase photogenerated current for optoelectronic devices.

Various applications require minimized reflection at particular wavelengths, which necessitates tuning the resonance of the nanostructures decorating the surface of the optoelectronic device in question. This tuning can be achieved by varying the spacing between the spheres (Figure 4a) or the diameter of the spheres (Figure 4b). As expected, increasing either the diameter or spacing between the spheres leads to a redshift of the resonances. Three particular resonances are emphasized in Figure 4, corresponding to resonances 1, 2, and 4 from Figure 2. The redshift is more pronounced as the diameter of the sphere is increased compared to that when an air-gap spacing layer is added to the lattice because the electric field experiences

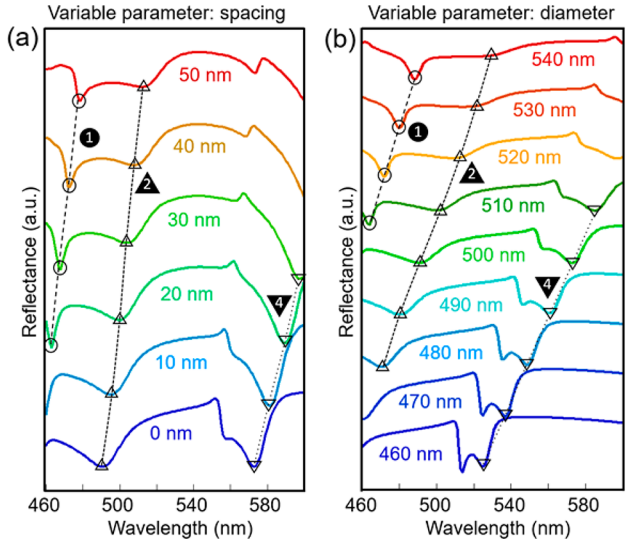

Figure 4. Reflectance as a function of wavelength for a monolayer of SiO_2 spheres on a Si substrate showing the reflectance variation due to (a) the spacing between the 500 nm diameter spheres and (b) the sphere diameter in a close-packed configuration. The three resonances (assigned as 1, 2, and 4) correspond to the resonances that occur at the normal incidence shown in Figure 2. The dashed lines are guides to the eye. All calculations are based on the FDTD method.

a higher effective index of refraction, resulting in a larger periodicity for electromagnetic waves within the layer.

To investigate the optical resonances in more detail experimentally, we measured the reflectance on the microscale regime using an upright optical microscope (Figure 5a). For

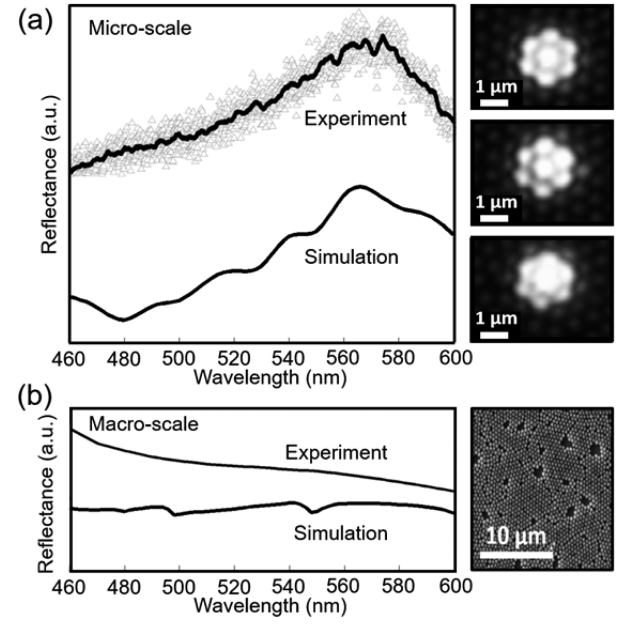

Figure 5. (a, left) Microscopic reflectance measurements and simulations for a set of close-packed SiO_2 nanospheres. (a, right) Representative optical images of three close-packed clusters under illumination. (b, left) Macroscopic reflectance measurements and simulations corresponding to an angle of incidence of 10° with respect to the normal. Measurements were performed using an integrating sphere and calculations were performed using the FDTD method. (b, right) SEM image showing SiO_2 nanospheres on top of a Si wafer where the measurements were performed.

DOI: 10.1021/acsami.6b05734
ACS Appl. Mater. Interfaces 2016, 8, 24536−24542

this measurement, regions containing only close-packed SiO_2 nanospheres were selected. Three representative areas are shown in Figure 5a, where each hexagonal pattern shows illumination of seven close-packed SiO_2 nanospheres. For normally incident light at λ = 573 nm, one would expect excitation of a whispering gallery-like mode and reduced reflection; however, Figure 5a instead shows a peak in the reflectance near this wavelength. This peak is caused by an angle averaging effect of the numerical aperture of the objective lens (NA = 0.75, corresponding to an acceptance angle of ~30°). As shown in Figure 2d, as the incident angle of illumination is increased from 0° to 30°, the resonance that occurs at λ = 573 nm is split (there is a red-shifted and a blue-shifted branch). FDTD simulations show that the weighted average of the reflectance over this angular region agrees well with the experimental results obtained via microscopic reflectance measurements (Figure 5a). For comparison, Figure 5b shows a macroscopic measurement of the reflectance obtained using an integrating sphere with a spot size of ~0.5 cm^2 at an incident angle of 10°. The relatively flat response is an effect of averaging over the resonances as a result of variation in sphere diameter, spacing, and periodicity/randomization, as seen in the SEM image (Figure 5b, right). Despite this averaging effect, simulations of the reflectance for a close-packed array of 500 nm diameter spheres illuminated at an incident angle of 10° describe the measurements well (Figure 5b, left). A weighted average of the reflectivity resulting from different sphere sizes based on SEM images results in a further flatting of the optical response (see Figure S3).

We performed local photocurrent measurements using a standard multicrystalline Si solar cell with a 75 nm thin-film silicon nitride (Si_3N_4) antireflection layer with and without the addition of the nanosphere coating (Figure 6). Light from a

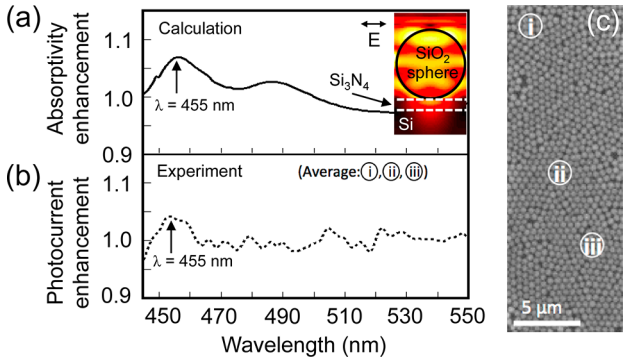

Figure 6. (a) Calculated absorptivity and (b) measured photocurrent enhancement resulting from the addition of a close-packed SiO_2 nanosphere coating to a planar Si solar cell that already contains a 75 nm Si_3N_4 ARC. Inset shows the calculated electric field profile at λ = 455 nm, which is similar to resonance 1 in Figure 2. A photocurrent enhancement of up to ~5% was measured. (c) SEM image showing three representative, close-packed regions where the measurements shown in panel b were performed.

supercontinuum laser was coupled into the scanning optical microscope to measure photogenerated current from the solar cell. The measured wavelength-dependent photocurrent of the device containing the nanosphere coating was normalized to the photocurrent obtained for the device without the coating. The average photocurrent enhancement obtained for three different regions with close-packed spheres is shown in Figure 6b. The measurement was compared with the calculated absorptivity enhancement based on FDTD simulations (Figure 6a). A peak in the calculated absorption and the measured photocurrent was found at λ = 455 nm. This peak corresponds to a resonance similar to that of resonance 1 (Figure 2d) for a SiO_2 array directly atop Si, whereas for the device in Figure 6, there is an additional Si_3N_4 coating. This resonance persists even though the incident illumination contains a range of angles (0–30°). The measured and calculated enhancements are found to be in good agreement. Figure 6c shows a SEM image of the closely packed nanosphere coating, indicating areas where the measurements were performed.

CONCLUSIONS

In conclusion, we developed SiO_2 dielectric nanosphere ARCs that improve light absorptivity within a semiconducting slab and ultimately increase the power conversion efficiency of solar cells by exploiting various optical resonances. A combination of optical simulations and experimental measurements were performed and compared, which enable insights into the excited modes. Photocurrent measurements for a Si solar cell were also presented, and the results illustrate how the excitation of individual modes can improve the optoelectronic properties of solar cells. Because the layer of SiO_2 nanospheres can be made with an easy, inexpensive, and scalable process, this type of ARC is an excellent new candidate for replacing conventional ARC technologies that are unsuitable for certain photovoltaic technologies.

METHODS

Deposition of SiO_2 Nanospheres. A monolayer of SiO_2 nanospheres was deposited on Si using the Meyer rod rolling technique with a 0.46 mm (0.018 in) wire wound rod (no. 18 wire wound rod, RD Specialties, Inc.). A surfactant (Zonyl) was added to the SiO_2 nanosphere suspension to prevent sphere agglomeration, resulting in a suspension with sphere concentration of ~0.1%. The coated sample was subjected to a mild annealing treatment at 50 °C for 1 min on a hot plate to evaporate the water.

Optical Measurements. For the macroscale reflection measurements, a 150 W xenon arc lamp (#6255, Newport Corp.) was coupled into a monochromator (500M, SPEX Industries, Inc.), and a 6 in. integrating sphere (Labsphere) was used. The samples were positioned in the center of the integrating sphere and rotated for the angle-dependent measurements using a two-port technique. The reflected light was collected by one Si photodetector attached at the bottom of the integrating sphere, while a second one monitored the incident power. The signal from these detectors were measured using a DSP lock-in amplifier (SR830, Stanford Research Systems). Error in the measurement technique was determined at wavelengths of interest (400–1100 nm) to be <1%.[46]

For the microscopic reflection measurements, a tungsten halogen white light source (BPS101, BWTEK Inc.) was connected to a confocal optical microscope via a multimode optical fiber. The reflection signal was recorded by a CCD camera (DV401-BV, WiTec). The reflection spectrum shown in Figure 5a is the average of 9 measurements for different regions of the sample with close-packed SiO_2 nanospheres, recorded with an integration time of 0.2 s per frame and an average over 100 frames.

Simulations of Optical Response. The FDTD method was used to simulate the optical response of the dielectric spheres (Lumerical FDTD Solutions). We assumed close-packed SiO_2 nanospheres on a Si substrate, and the absorptivity of the Si substrate was calculated from its reflection. We applied periodic boundary conditions horizontally within the simulated volume (or a Bloch boundary condition when a plane wave source was propagating at an angle) to simulate a periodic structure, and a perfectly matched layer boundary

DOI: 10.1021/acsami.6b05734
ACS Appl. Mater. Interfaces 2016, 8, 24536–24542

condition was used at the bottom of a Si substrate. Optical constants required for simulations were obtained from ref 47.

Optoelectronic Response Measurements. A confocal optical microscope was used for the photocurrent measurements, and a 100× objective lens was used as the local source of excitation (with NA = 0.75). The illumination source originated from a supercontinuum laser that was fiber-coupled to the microscope. Because the tunable laser has a nonuniform power spectrum, all measurements were normalized to the incident power for each wavelength.

■ ASSOCIATED CONTENT

Supporting Information

The Supporting Information is available free of charge on the ACS Publications website at DOI: 10.1021/acsami.6b05734.

Details regarding thin-film optical effects, SiO_2 nanosphere size variation, optical simulations of nonuniform arrays of SiO_2 nanospheres, and optimizations of Si solar cell structures with combined Si_3N_4 thin-film ARCs and SiO_2 nanosphere arrays (PDF)

■ AUTHOR INFORMATION

Corresponding Author

*E-mail: jnmunday@umd.edu.

Author Contributions

J.N.M. supervised the project. D.H. made samples and conducted the macroscale optical experiments and FDTD calculations. D.H. and C.G. performed microscale reflection and photocurrent measurements. All authors contributed to data analysis and this manuscript.

Notes

The authors declare no competing financial interest.

■ ACKNOWLEDGMENTS

The authors acknowledge Z. Fang and L. Hu for advice about the Meyer rod coating process, J. Murray for his technical assistance, and financial support from the University of Maryland. D.H. acknowledges support from the Graduate Dean's Dissertation Fellowship and the Future Faculty Program at the University of Maryland.

■ REFERENCES

(1) Zhao, J.; Green, M. A. Optimized Antireflection Coatings for High-Efficiency Silicon Solar Cells. *IEEE Trans. Electron Devices* **1991**, *38*, 1925−1934.

(2) Zhao, J.; Wang, A.; Altermatt, P.; Green, M. A. Twenty-Four Percent Efficient Silicon Solar Cells with Double Layer Antireflection Coatings and Reduced Resistance Loss. *Appl. Phys. Lett.* **1995**, *66*, 3636−3638.

(3) Richards, B. S. Single-Material TiO_2 Double-Layer Antireflection Coatings. *Sol. Energy Mater. Sol. Cells* **2003**, *79*, 369−390.

(4) Aroutiounian, V. M.; Martirosyan, Kh.; Soukiassian, P. Almost Zero Reflectance of a Silicon Oxynitride/Porous Silicon Double Layer Antireflection Coating for Silicon Photovoltaic Cells. *J. Phys. D: Appl. Phys.* **2006**, *39*, 1623−1625.

(5) Ferry, V. E.; Munday, J. N.; Atwater, H. A. Design Considerations for Plasmonic Photovoltaics. *Adv. Mater.* **2010**, *22*, 4794−4808.

(6) Atwater, H. A.; Polman, A. Plasmonics for Improved Photovoltaic Devices. *Nat. Mater.* **2010**, *9*, 205−213.

(7) Stuart, H. R.; Hall, D. G. Island Size Effects in Nanoparticle-Enhanced Photodetectors. *Appl. Phys. Lett.* **1998**, *73*, 3815−3817.

(8) Munday, J. N.; Atwater, H. A. Large Integrated Absorption Enhancement in Plasmonic Solar Cells by Combining Metallic Gratings and Antireflection Coatings. *Nano Lett.* **2011**, *11*, 2195−2201.

(9) Atwater, H. A.; Polman, A. Plasmonics for Improved Photovoltaic Devices. *Nat. Mater.* **2010**, *9*, 205−213.

(10) Catchpole, K. R.; Polman, A. Design Principles for Particle Plasmon Enhanced Solar Cells. *Appl. Phys. Lett.* **2008**, *93*, 191113.

(11) Catchpole, K. R.; Polman, A. Plasmonic Solar Cells. *Opt. Express* **2008**, *16*, 21793−21800.

(12) Gan, Q.; Bartoli, F. J.; Kafafi, Z. H. Plasmonic-Enhanced Organic Photovoltaics: Breaking the 10% Efficiency Barrier. *Adv. Mater.* **2013**, *25*, 2385−2396.

(13) Ding, I. K.; Zhu, J.; Cai, W.; Moon, S.-J.; Cai, N.; Wang, P.; Zakeeruddin, S. M.; Gratzel, M.; Brongersma, M. L.; Cui, Y.; McGehee, M. D. Plasmonic Dye-Sensitized Solar Cells. *Adv. Energy Mater.* **2011**, *1*, 52−57.

(14) Bhattacharya, J.; Chakravarty, N.; Pattnaik, S.; Slafer, W. D.; Biswas, R.; Dalal, V. L. A Photonic-Plasmonic Structure for Enhancing Light Absorption in Thin Film Solar Cells. *Appl. Phys. Lett.* **2011**, *99*, 131114.

(15) Pala, R. A.; White, J.; Barnard, E.; Liu, J.; Brongersma, M. L. Design of Plasmonic Thin-Film Solar Cells with Broadband Absorption Enhancements. *Adv. Mater.* **2009**, *21*, 3504−3509.

(16) Hägglund, C.; Zäch, M.; Petersson, G.; Kasemo, B. Electromagnetic Coupling of Light into a Silicon Solar Cell by Nanodisk Plasmons. *Appl. Phys. Lett.* **2008**, *92*, 053110.

(17) Dabirian, A.; Byranvand, M. M.; Naqavi, A.; Kharat, A. N.; Taghavinia, N. Self-Assembled Monolayer of Wavelength-Scale Core−Shell Particles for Low-Loss Plasmonic and Broadband Light Trapping in Solar Cells. *ACS Appl. Mater. Interfaces* **2016**, *8*, 247−255.

(18) Spinelli, P.; Verschuuren, M. A.; Polman, A. Broadband Omnidirectional Antireflection Coating Based on Subwavelength Surface Mie Resonators. *Nat. Commun.* **2012**, *3*, 692.

(19) Brongersma, M. L.; Cui, Y.; Fan, S. Light Management for Photovoltaics Using High-Index Nanostructures. *Nat. Mater.* **2014**, *13*, 451−460.

(20) Grandidier, J.; Callahan, D. M.; Munday, J. N.; Atwater, H. A. Light Absorption Enhancement in Thin-Film Solar Cells Using Whispering Gallery Modes in Dielectric Nanospheres. *Adv. Mater.* **2011**, *23*, 1272−1276.

(21) Grandidier, J.; Callahan, D. M.; Munday, J. N.; Atwater, H. A. Gallium Arsenide Solar Cell Absorption Enhancement Using Whispering Gallery Modes of Dielectric Nanospheres. *IEEE J. Photovoltaics* **2012**, *2*, 123−128.

(22) Grandidier, J.; Weitekamp, R. A.; Deceglie, M. G.; Callahan, D. M.; Battaglia, C.; Bukowsky, C. R.; Ballif, C.; Grubbs, R. H.; Atwater, H. A. Solar Cell Efficiency Enhancement Via Light Trapping in Printable Resonant Dielectric Nanosphere Arrays. *Phys. Status Solidi A* **2013**, *210*, 255−260.

(23) Yariv, A.; Xu, Y.; Lee, R. K.; Scherer, A. Coupled-Resonator Optical Waveguide: A Proposal and Analysis. *Opt. Lett.* **1999**, *24*, 711−713.

(24) Derkacs, D.; Chen, W. V.; Matheu, P. M.; Lim, S. H.; Yu, P. K. L.; Yu, E. T. Nanoparticle-Induced Light Scattering for Improved Performance of Quantum-Well Solar Cells. *Appl. Phys. Lett.* **2008**, *93*, 091107.

(25) Zhu, J.; Hsu, C.-M.; Yu, Z.; Fan, S.; Cui, Y. Nanodome Solar Cells with Efficient Light Management and Self-Cleaning. *Nano Lett.* **2010**, *10*, 1979−1984.

(26) Kroll, M.; Fahr, S.; Helgert, C.; Rockstuhl, C.; Lederer, F.; Pertsch, T. Employing Dielectric Diffractive Structures in Solar Cells − A Numerical Study. *Phys. Status Solidi A* **2008**, *205*, 2777−2795.

(27) Dabirian, A.; Taghavinia, N. Resonant-Size Spherical Bottom Scatterers for Dye-Sensitized Solar Cells. *RSC Adv.* **2013**, *3*, 25417−25422.

(28) Ein-Eli, Y.; Gordon, N.; Starosvetsky, D. Reduced Light Reflection of Textured Multicrystalline Silicon via NPD for Solar Cells Applications. *Sol. Energy Mater. Sol. Cells* **2006**, *90*, 1764−1772.

(29) Ha, D.; Fang, Z.; Hu, L.; Munday, J. N. Paper-Based Anti-Reflection Coatings for Photovoltaics. *Adv. Energy. Mater.* **2014**, *4*, 1301804.

(30) Ha, D.; Murray, J.; Fang, Z.; Hu, L.; Munday, J. N. Advanced Broadband Antireflection Coatings Based on Cellulose Microfiber Paper. *IEEE J. Photovoltaics* **2015**, *5*, 577−583.
(31) Hsu, C.-M.; Connor, S. T.; Tang, M. X.; Cui, Y. Wafer-Scale Silicon Nanopillars and Nanocones by Langmuir−Blodgett Assembly and Etching. *Appl. Phys. Lett.* **2008**, *93*, 133109.
(32) Jiang, P.; Bertone, J. F.; Hwang, K. S.; Colvin, V. L. Single-Crystal Colloidal Multilayers of Controlled Thickness. *Chem. Mater.* **1999**, *11*, 2132−2140.
(33) Mihi, A.; Zhang, C.; Braun, P. V. Transfer of Preformed 3D Photonic Crystals onto Dye Sensitized Solar Cells. *Angew. Chem., Int. Ed.* **2011**, *50*, 5712−5715.
(34) Wang, J.; Liang, M.; Fang, Y.; Qiu, T.; Zhang, J.; Zhi, L. Rod-Coating: Towards Large-Area Fabrication of Uniform Reduced Graphene Oxide Films for Flexible Touch Screens. *Adv. Mater.* **2012**, *24*, 2874−2878.
(35) Hu, L.; Kim, H. S.; Lee, J.-Y.; Peumans, P.; Cui, Y. Scalable Coating and Properties of Transparent, Flexible, Silver Nanowire Electrodes. *ACS Nano* **2010**, *4*, 2955−2963.
(36) Dan, B.; Irvin, G. C.; Pasquali, M. Continuous and Scalable Fabrication of Transparent Conducting Carbon Nanotube Films. *ACS Nano* **2009**, *3*, 835−843.
(37) Yin, J.; Zang, Y.; Yue, C.; He, X.; Li, J.; Wu, Z.; Fang, Y. Self-Assembled Hollow Nanosphere Arrays Used as Low Q Whispering Gallery Mode Resonators on Thin Film Solar Cells for Light Trapping. *Phys. Chem. Chem. Phys.* **2013**, *15*, 16874−16882.
(38) Mariano, M.; Rodríguez, F. J.; Romero-Gomez, P.; Kozyreff, G.; Martorell, J. Light Coupling into The Whispering Gallery Modes of a Fiber Array Thin Film Solar Cell for Fixed Partial Sun Tracking. *Sci. Rep.* **2014**, *4*, 4959.
(39) Yao, Y.; Yao, J.; Narasimhan, V. K.; Ruan, Z.; Xie, C.; Fan, S.; Cui, Y. Broadband Light Management Using Low-Q Whispering Gallery Modes in Spherical Nanoshells. *Nat. Commun.* **2012**, *3*, 664.
(40) Cole, R. M.; Sugawara, Y.; Baumberg, J. J.; Mahajan, S.; Abdelsalam, M.; Bartlett, P. N. Easily Coupled Whispering Gallery Plasmons in Dielectric Nanospheres Embedded in Gold Films. *Phys. Rev. Lett.* **2006**, *97*, 137401.
(41) Hayata, K.; Yénaka, H.; Koshiba, M. Theory of Coherent Optical Coupling Between Dielectric Microspheres. *Opt. Lett.* **1993**, *18*, 1385−1387.
(42) Yu, X.; Shi, L.; Han, D.; Zi, J.; Braun, P. V. High Quality Factor Metallodielectric Hybrid Plasmonic-Photonic Crystals. *Adv. Funct. Mater.* **2010**, *20*, 1910−1916.
(43) le Floch, J.-M.; Anstie, J. D.; Tobar, M. E.; Hartnett, J. G.; Bourgeois, P.-Y.; Cros, D. Whispering Modes in Anisotropic and Isotropic Dielectric Spherical Resonators. *Phys. Lett. A* **2006**, *359*, 1−7.
(44) McCall, S. L.; Levi, A. F. J.; Slusher, R. E.; Pearton, S. J.; Logan, R. A. Whispering-gallery Mode Microdisk Lasers. *Appl. Phys. Lett.* **1992**, *60*, 289−291.
(45) Cai, M.; Painter, O.; Vahala, K. J. Observation of Critical Coupling in a Fiber Taper to a Silica-Microsphere Whispering-Gallery Mode System. *Phys. Rev. Lett.* **2000**, *85*, 74−77.
(46) Murray, J. Experimental Investigation of Light Trapping and Internal Light Scattering in Solar Cells. Ph.D. Thesis, The University of Maryland, College Park, MD, April 2016.
(47) Palik, E. D. *Handbook of Optical Constants of Solids*, 1st ed.; Academic Press: Cambridge, 1997.

DOI: 10.1021/acsami.6b05734
ACS Appl. Mater. Interfaces 2016, 8, 24536−24542